RSC Advances

PAPER

View Article Online
View Journal | View Issue

Cite this: *RSC Adv.*, 2026, **16**, 19128

Green carbon dots-embedded polymeric membranes for simultaneous photocatalytic dye degradation and antibacterial activity

Alejandro López Amador,[a] Pamela Ortega Sánchez,[b] Arlete Yuriana Vázquez García,[a] Jesús Adrián Díaz Real,[a] Ángel de Jesús Montes Luna,[c] Noé Arjona,[d] Gabriel Luna Bárcenas[e] and Beatriz Liliana España Sánchez *[e]

This work presents the development of multifunctional polymeric membranes incorporating green-synthesized carbon dots (CDs) that simultaneously enable the photodegradation of methylene blue (MB) and exhibit antibacterial activity. CDs containing nitrogen and oxygen heteroatoms were synthesized from natural precursors and embedded into hydrophilic (PVA/PAA) and hydrophobic (PPSU) polymeric matrices *via* a phase-inversion method. The physicochemical properties of the membranes were characterized by FTIR and SEM, revealing changes in chemical interactions, morphology, and porosity induced by CD incorporation. The resulting nanostructured membranes exhibited enhanced photocatalytic performance under light irradiation, achieving rapid dye removal within the first 24 h and promoting advanced oxidation of MB, as supported by chemical oxygen demand (COD) analysis. In addition, the membranes demonstrated strong antibacterial activity against representative Gram-positive and Gram-negative bacteria, with high inhibition efficiency maintained under simultaneous photocatalytic conditions. The improved performance is attributed to the photoactive nature of CDs, their ability to generate reactive oxygen species, and their interactions with the polymer matrices. Overall, this study demonstrates that green-synthesized CD-based membranes represent an effective and sustainable strategy for integrated pollutant degradation and microbial control in water treatment applications.

Received 4th February 2026
Accepted 30th March 2026

DOI: 10.1039/d6ra00999a

rsc.li/rsc-advances

1. Introduction

Water pollution has emerged as a critical global challenge, driven by the continuous discharge of anthropogenic contaminants into rivers and groundwater systems. Among these pollutants, synthetic dyes (primarily released from the textile and leather industries) are of particular concern due to their high chemical stability, persistence in aquatic environments, and detrimental effects on flora and fauna. Methylene blue (MB), a synthetic dye widely employed in the textile, paper, and pharmaceutical industries, has become a major source of water pollution.[1] Due to its high solubility and stability, MB is difficult to remove by conventional treatments and persists in the environment, adversely affecting both water quality and aquatic life. Moreover, its presence at elevated concentrations can induce toxic effects in aquatic organisms and pose a potential risk to human health.[2,3] Therefore, the efficient removal of this compound has emerged as a crucial challenge in industrial wastewater treatment.

In this context, nanostructured polymeric membranes have emerged as a promising alternative, offering advantages such as high selectivity and enhanced degradation capacity.[4] Membranes employed for dye photodegradation encompass a wide range of configurations and compositions, specifically engineered to integrate both separation and photocatalytic functions, owing to their versatility, ease of processing, and compatibility with photocatalytic nanomaterials.[5] Among these, hydrophilic polymers such as polyvinyl alcohol (PVA) and polyacrylic acid (PAA) have proven to be efficient matrices for the incorporation of semiconductor oxides (*e.g.*, CDs, TiO_2, ZnO, or $BiVO_4$),[6,7] owing to their strong water affinity, good mechanical stability, and ability to form crosslinked networks that enhance nanoparticle dispersion, thereby optimizing light-induced photocatalytic pollutant interactions. Similarly,

[a]*Centro de Investigación y Desarrollo Tecnológico en Electroquímica CIDETEQ SC., Parque Tecnológico Querétaro s/n, Sanfandila, Pedro Escobedo, Querétaro C. P. 76703, Mexico*

[b]*Centro de Investigación, Universidad Anáhuac Querétaro, El Marqués, Querétaro 76246, Mexico*

[c]*Unidad de Materiales, Centro de Investigación Científica de Yucatán, Mérida, C. P. 97205, Mexico*

[d]*Centro de Investigación en Materiales Avanzados S.C., Complejo Industrial Chihuahua, Chihuahua Chih., C. P. 311136, Mexico*

[e]*Tecnologico de Monterrey, Institute of Advanced Materials for Sustainable Manufacturing, Epigmenio González 500 Fracc. San Pablo, Qro, Santiago de Querétaro, C. P. 76130, Mexico. E-mail: liliana.espana@tec.mx*

polyphenylsulfone (PPSU) has been established as a robust, chemically resistant polymeric matrix, particularly suitable for applications under harsh conditions, thereby enabling the stable immobilization of photocatalysts without compromising the membrane's structural integrity.[8]

Among emerging nanomaterials, carbon dots (CDs) have attracted significant attention for photocatalytic pollutant degradation and water treatment applications due to their tunable optical properties, low toxicity, and high surface functionality.[9] These nanomaterials exhibit strong light absorption, efficient charge separation, and the ability to generate reactive oxygen species (ROS), which are essential for oxidative degradation processes.[10] Recent studies have demonstrated that CD-based systems, including hybrid membranes and heteroatom-doped CDs, can significantly enhance photocatalytic performance under visible-light irradiation, thereby improving dye degradation efficiency and operational stability. In particular, heteroatom doping (*e.g.*, nitrogen and oxygen) introduces surface defect states that facilitate charge transfer and ROS generation, thereby boosting photoreactivity.[11,12]

Despite these advances, most reported CD-based photocatalytic systems primarily focus on single-function applications, particularly pollutant degradation under controlled irradiation conditions.[13] In contrast, limited attention has been given to multifunctional systems capable of simultaneously addressing organic pollutants and microbial contamination under realistic conditions.[14] Additionally, many reported approaches rely on synthetic precursors or complex fabrication strategies, which may limit their environmental compatibility and scalability.[11,14] Therefore, the development of sustainable, multifunctional systems based on green-synthesized CDs represents a relevant research opportunity.

The incorporation of CDs into photocatalytic membranes has emerged as a highly promising strategy for the efficient degradation of dyes in aqueous media, owing to their photoactive properties and ability to interact with a wide variety of chemical and biological species.[15] These nanomaterials, characterized by sizes below 10 nm and high surface functionality, significantly enhance light absorption and promote electron–hole separation while maintaining excellent compatibility with both polymeric and ceramic matrices. Recent studies have demonstrated that the impregnation of CDs into membranes confers improved properties, including enhanced photocatalytic activity, thermal stability, and efficiency in the degradation of methylene blue under illumination.[16]

Photocatalytic degradation of MB supported on membranes is an effective strategy for removing this contaminant from aqueous media, leveraging the synergy between selective dye adsorption and the nanomaterial's photocatalytic activity. Furthermore, this approach endows the membranes with self-cleaning properties and extends their operational lifespan, thereby reducing the overall costs of wastewater treatment.[17] In this work, multifunctional nanostructured membranes incorporating green-synthesized carbon dots derived from natural sources are developed using PVA/PAA and PPSU polymeric matrices. The study systematically evaluates the influence of polymeric environment (hydrophilic *vs.* hydrophobic) on photocatalytic performance, as well as the role of CDs in enhancing both dye degradation and antibacterial activity. Additionally, the performance of the membranes is assessed under natural solar irradiation, providing a more realistic evaluation than conventional studies using artificial light sources. This work provides new insights into the synergistic interaction between CDs and polymeric matrices, contributing to the design of sustainable and efficient materials for water treatment applications.

2. Experimental

2.1. Synthesis of CDs by green sources

The synthesis of CDs was performed as described in our previous report.[18] Briefly, a mixture was prepared from three natural precursors: lemon juice, aloe vera pulp, and green tea infusion. The aloe vera pulp was first homogenized together with the lemon juice, after which both were incorporated into the green tea infusion. The resulting mixture was transferred to a hydrothermal reactor and heated at 200 °C for 6 h (patent request MX/a/2025/002403) to synthesize carbon dots. To determine the morphology of CDs, high-resolution transmission electron microscopy (HRTEM) analyses were performed using a JEOL JEM-2200FS+CS microscope, equipped with a tungsten filament and operated at 200 kV. The chemical composition of CDs and nanostructured membranes was determined using Fourier transform infrared (FTIR) spectroscopy. Measurements were performed using a PerkinElmer instrument equipped with an ATR accessory. Spectra were recorded over the range of 4000–400 cm^{-1}, with 20 scans at a resolution of 4 cm^{-1}. Fluorescence measurements of aqueous CD solutions were performed in a quartz cuvette using a spectrophotometer (Agilent Cary Eclipse) with excitation at different wavelengths. Emission spectra were recorded from 330 to 390 nm. Dynamic light scattering (DLS) measurements were conducted with CDs in solution using an Anton Paar Litesizer 500 particle analyzer.

2.2. Fabrication of nanostructured membranes

Polyvinyl alcohol (PVA, M_w 89 000–98 000, 99% hydrolyzed) and polyacrylic acid (PAA, M_v 450 000) were purchased from Sigma-Aldrich. To compare the performance of common polymers used in water filtration, polyphenylsulfone (PPSU, Radel-5550®) was purchased from Sigma-Aldrich. For this purpose, two types of membranes were prepared: the first was based on a polymeric matrix composed of polyvinyl alcohol (PVA) and polyacrylic acid (PAA). They were used in a 2 : 1 ratio, corresponding to concentrations of 10 wt% and 5 wt%, respectively, while the second used polyphenylsulfone (PPSU) at 12% p/p in dimethylformamide (DMF). In both cases, the CDs were incorporated during membrane fabrication, which was carried out by phase inversion *via* solvent exchange, with distilled water as the nonsolvent. Once the membranes were obtained, they were cross-linked in an oven at 120 °C for 3 hours.

To evaluate the morphology of PVA/PAA and PPSU upon the addition of CDs, SEM micrographs were obtained using a JEOL

JSM-6610LV. The analysis was performed at the surface of each sample, and a cryogenic fracture was obtained to analyze the transversal section of each membrane. To calculate the porosity of each membrane (ε), defined as the ratio between the pore volume and the total volume of the porous membrane, gravimetric measurements of the retained water were performed, according to eqn (1), based on the gravimetric method commonly used for porous membranes[19]

$$\varepsilon = \frac{\frac{(w_1 - w_2)}{d_w}}{\frac{(w_1 - w_2)}{d_w} + \frac{w_2}{d_p}} \times 100 \quad (1)$$

where w_1 represents the weight of the wet membrane, w_2 is the weight of the dry membrane, d_w is the density of pure water (0.998 g cm^{-3}), and d_p is the density of the polymer (1.31 g cm^{-3} for PPSU and 1.28 g cm^{-3} for PVA/PAA, respectively).

2.3. Photodegradation assays

Photodegradation experiments were carried out using MB as a model contaminant at initial concentrations of 2, 4, 6, 8, and 10 ppm. For each experiment, membrane fragments measuring 1 × 1 cm^2 were prepared and brought into contact with 10 mL of the dye solutions at the predetermined concentrations. Each system was placed in a sealed vial containing the MB solution and the membrane fragment, then exposed to natural solar radiation by positioning the vials on a window facing direct sunlight. The photodegradation process was monitored over 7 days, with the solution's absorbance measured periodically to assess the rate of dye degradation. Methylene blue degradation was monitored in a quartz cell using a BK-UV1800PC spectrophotometer, with scans from 200 to 800 nm. For each measurement, a 1 mL aliquot was withdrawn directly from the vial, analyzed, and returned to the system, maintaining a constant total volume. Additionally, dark control experiments were performed using the same procedure, except that the vials were kept completely shielded from solar light. Likewise, during absorbance measurements, the vials were adequately covered to prevent interference from accidental sunlight exposure.

The photocatalytic degradation kinetics of methylene blue were analyzed using a pseudo-first-order model based on the Langmuir–Hinshelwood approach, according to:

$$\ln\left(\frac{C_0}{C_t}\right) = kt \quad (2)$$

where C_0 and C_t are the dye concentrations at initial time and time t, respectively, and k is the apparent rate constant.[20]

To investigate the potential involvement of reactive oxygen species (ROS) in the photocatalytic degradation of methylene blue (MB), experiments were conducted with scavenging agents, including isopropanol (IPA) as a neutralizer of the hydroxyl radical ($^{\bullet}$OH). A defined volume of IPA (100 μL) was added to the MB solution before the membrane was introduced. Experimental conditions (MB concentration, solution volume, membrane size, and light exposure) were maintained identically to those used in the photocatalytic degradation experiments. The degradation process was monitored by UV-Vis spectroscopy under the same conditions, and the results were compared with control experiments performed in the absence of IPA.[21]

2.4. Chemical oxygen demand (COD) assays

Chemical oxygen demand (COD) measurements were performed using the reactor digestion method, employing high-range COD digestion vials (20–1500 mg L^{-1}), a HACH DRB200 digestion reactor, and a HACH DR 6000 spectrophotometer. The procedure was performed in accordance with Standard Method 5220D.[22] Briefly, 2 mL of each sample was added to the digestion vials (deionized water as the blank). The vials were sealed, gently shaken, and then heated to 150 °C for 2 h. After digestion, the vials were cooled to room temperature. COD was determined spectrophotometrically at 620 nm, beginning with the blank, then the samples, and the final COD values were expressed as percentages (%).

2.5. Antibacterial performance

For the antibacterial assays, Gram-positive *Staphylococcus aureus* (ATCC No. 6538) and Gram-negative *Pseudomonas aeruginosa* (ATCC No. 13388) strains were cultured in Luria-Bertani (LB) broth. Membrane testing was conducted in accordance with ASTM E2149, "Standard Test Method for Determining the Antimicrobial Activity of Antimicrobial Agents Under Dynamic Contact Conditions," with slight adaptations, using 1 cm^2 of membrane per test. The bacterial inoculum of *S. aureus* and *P. aeruginosa* was adjusted to 1 × 10^5 colony-forming units (CFU mL^{-1}). Antibacterial tests were performed at different contact times (1, 3, and 24 hours) and incubated at 37 °C. After incubation, a 50 μL aliquot was plated onto LB agar and incubated for 16 hours at 37 °C.

The antibacterial activity (AA) percentage was calculated using the following equation, according to the approaches described in the literature[23]

$$\mathrm{AA} = \left(\frac{\mathrm{Control} - \mathrm{sample}}{\mathrm{Control}}\right) \times 100 \quad (3)$$

3. Results and discussion

3.1. Green synthesis of CDs

The green synthesis of CDs was performed *via* the hydrothermal method, using a mixture of natural sources (*aloe vera*, lemon juice, and green tea), as described in our previous work.[18] The CDs characterization is shown in Fig. 1. Fig. 1a shows representative HRTEM micrographs of CDs, revealing quasi-spherical particles with diameters ranging from 6 to 30 nm, with the most frequent distribution between 14 and 18 nm. These clusters are attributed to solvent evaporation during sample preparation used to obtain the powder 14, a characteristic of CDs obtained from natural sources such as leaves, biomass, and lemon juice 15–17, indicating amorphous carbon degradation during the hydrothermal process and the role of

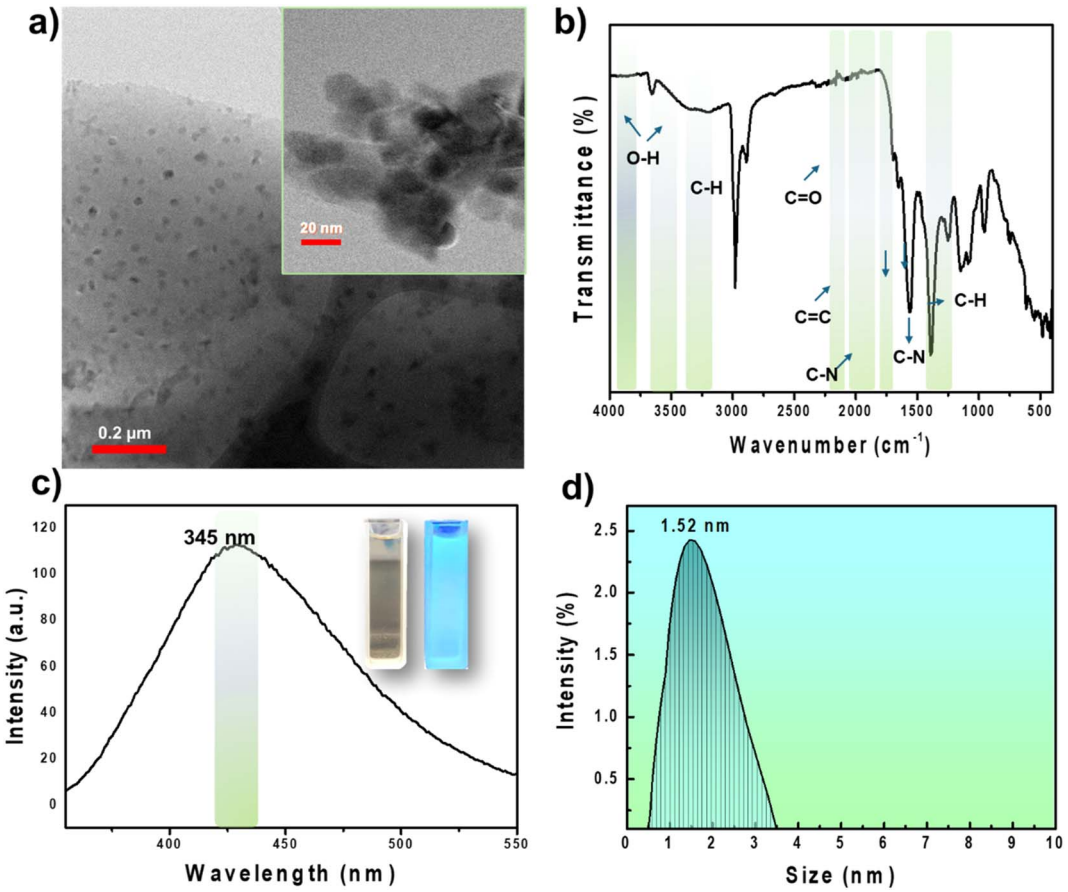

Fig. 1 Physicochemical characterization of carbon dots (CDs) synthesized from natural sources. (a) HRTEM micrographs showing quasi-spherical morphology and particle size distribution. (b) FTIR spectrum indicating the presence of oxygen- and nitrogen-containing functional groups. (c) UV-Vis absorption and photoluminescence (PL) spectra, along with digital photographs under visible and UV light, demonstrating blue emission. (d) Dynamic light scattering (DLS) analysis showing the hydrodynamic size distribution of CDs in aqueous dispersion.

the organic composition in the formation of CDs. FTIR measurements of the CDs powder demonstrate the chemical composition induced by the natural source, as shown in Fig. 1b. The spectrum revealed several characteristic absorption bands. A broad signal around 3257 cm^{-1} corresponds to the stretching vibrations of O–H and N–H groups, which are associated with enhanced water solubility and stability in aqueous media. The bands located at 2978, 2879, 956, 730, and 621 cm^{-1} are attributed to C–H bending vibrations, suggesting the presence of methyl or methylene groups.[24] The band at 1700 cm^{-1} corresponds to the C=O stretching vibration, indicative of functional groups such as ketones, aldehydes, or carboxylic acids. Additionally, the signals at 1664 and 1563 cm^{-1} are assigned to C=C stretching vibrations, suggesting the presence of conjugated double-bond structures.[25] The bands observed at 1384, 1246, and 1070 cm^{-1} are attributed to C–N stretching vibrations, indicating the possible presence of amine, amide, or nitrile groups. Finally, the band at 1146 cm^{-1} corresponds to the C–O stretching vibration, suggesting the presence of ether, ester, or alcohol groups,[26] indicating the presence of heteroatoms at the surface of CDs, consistent with previous reports.[27–30] Photoluminescence (PL) spectra presented in Fig. 1c indicate that the CDs exhibit a maximum emission intensity at 428 nm, characteristic of blue emission in the visible spectrum. This behavior suggests that the crystalline size of the CDs falls within the typical range associated with this type of emission.[31] Furthermore, the observed emission may be attributable to carbon functional groups bearing heteroatoms, such as nitrogen and oxygen, incorporated into the CDs' structure.[32] This distinctive feature arises from energy states associated with surface defects of the nanoparticles.[33] One of the most widely accepted fluorescence mechanisms in CDs is attributed to their surface states, which encompass the oxidation level and the nature of the functional groups present on their surface.[34] To corroborate the effect of the CDs dispersion in water, DLS measurements were performed (Fig. 1d), allowing evaluation of the hydrodynamic size of the particles in colloidal media and assessment of their stability by detecting potential aggregation or agglomeration processes. The resulting spectrum shows a broad size distribution with an average particle size of 1.52 nm. This discrepancy, when compared to the sizes observed by HRTEM, confirms the presence of aggregates in the solid state and the lack of particle uniformity. Such heterogeneity is a common limitation in the synthesis of CDs from natural sources using green chemistry methods.

3.2. Physicochemical behavior of nanostructured membranes

Fig. 2 shows the FTIR spectra of the pristine PVA/PAA and PVA/PAA-CDs membranes, which display the characteristic bands of both polymers and variations induced by CDs incorporation into the polymeric matrix. As expected, characteristic vibrational bands corresponding to C=O, C=C, C–N, C–C, and C–H bonds inherent to PVA and PAA were identified, located within the 400–1750 cm^{-1} region. These signals are attributed to bending and stretching modes associated with these bonds, in good agreement with those reported in the literature for these polymers.[35] After the incorporation of CDs, the spectrum retains the main structural signals of the PVA/PAA matrix, indicating that the inclusion of CDs does not chemically alter the polymer backbone. However, a broadening and increase in the intensity of the –OH band (~3300 cm^{-1}) are observed, indicating interaction between the hydroxyl and carboxyl surface groups of the CDs and the polymeric chains *via* hydrogen bonding. Likewise, a slight shift toward lower wavenumbers in the C=O peak (~1720 cm^{-1}) indicates electrostatic interactions or partial bond formation between the carbonyl groups of PAA and the oxygen-containing functional groups of the CDs. This behavior indicates that the organic source of CDs and their chemical composition play a key role in their interactions with membranes during processing, consistent with ref. 36 and 37.

The morphological arrangement of PVA/PAA and PVA/PAA-CDs membranes was determined from SEM micrographs, as shown in the scheme of surface (Fig. 2b and c), and the transversal section (Fig. 2d and e), respectively. The pristine PVA/PAA surface (Fig. 2b) shows a homogeneous, continuous, and defect-free morphology, exhibiting a smooth topography characteristic of well-compatibilized polymer blends.[38] The absence of cracks, aggregates, or irregularities suggests good miscibility between

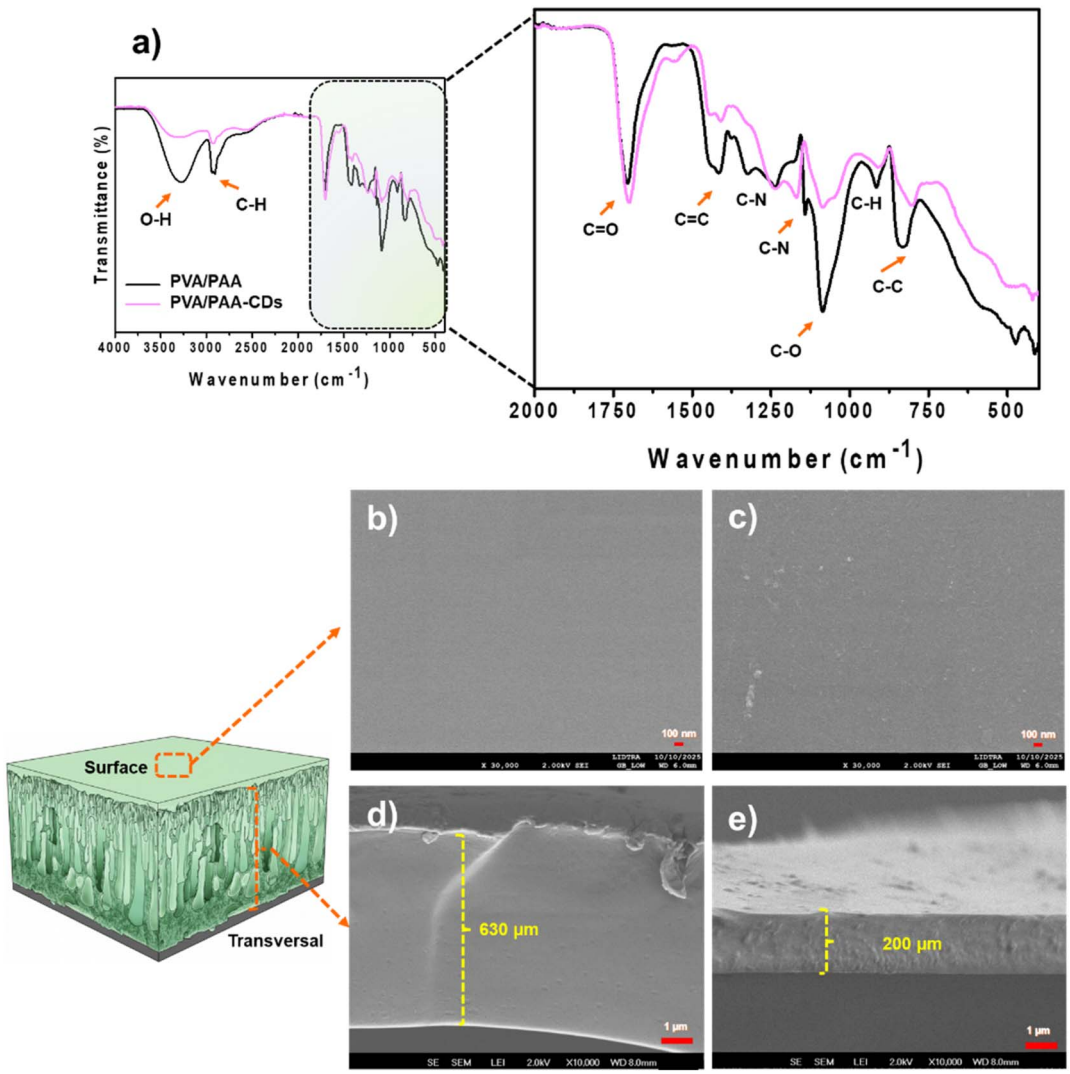

Fig. 2 Chemical and morphological characterization of PVA/PAA membranes and the effect of CDs incorporation. (a) FTIR spectra with zoomed region (2000–400 cm^{-1}) highlighting changes in functional groups due to CDs. (b and c) Surface SEM micrographs of pristine PVA/PAA and PVA/PAA-CDs membranes, respectively, showing morphological differences and CD dispersion. (d and e) Cross-sectional SEM images obtained by cryogenic fracture, illustrating membrane thickness and internal structure.

the PVA and PAA chains, consistent with hydrogen bonding between the hydroxyl and carboxyl groups of both components. In contrast, the surface of the PVA/PAA-CDs membrane (Fig. 2c) exhibits slight textural variations, with microdomains or bright spots uniformly distributed across the surface, which can be attributed to CDs either embedded within the membrane or partially exposed at the surface. Although the material maintains its structural integrity, these surface irregularities indicate that the incorporation of CDs induces local morphological modifications, suggesting physical interactions between the oxygen-containing functional groups of the CDs and the polymeric chains. These interactions, likely hydrogen bonding or π–π stacking, may increase surface energy and slightly increase roughness without compromising the material's continuity. Additionally, the absence of large aggregates or fractures indicates good dispersion of CDs within the matrix, facilitated by the chemical affinity between the hydroxyl and carboxyl groups of PVA/PAA and the surface functional species of the CDs.[33,38] Similar behavior was observed in the transverse section of the pristine membrane (Fig. 2d), showing a homogeneous thickness of approximately 630 μm.

To compare the effects of incorporating CDs into high-performance polymers for water filtration, PPSU was used as a model system, as shown in Fig. 3. Both spectra exhibit the characteristic bands of the base polymer (Fig. 3a), confirming that the matrix's chemical structure remains largely unaffected by CDs incorporation. However, a slight broadening and decrease in transmittance are observed in the 3400–3200 cm^{-1} region, which may be associated with surface hydroxyl (–OH) groups originating from the CDs. Additionally, slight modifications in the intensity of the bands around 1650–1600 cm^{-1} can be attributed to C═O or conjugated C═C vibrations from the CDs framework. These variations suggest the presence of intermolecular interactions, such as hydrogen bonding or π–π interactions between the aromatic domains of the polymer and the oxygen-containing functional groups of the CDs.[39,40]

The slight variations in surface texture observed in the PVA/PAA-CDs membranes do not adversely affect their performance and are mainly associated with the intrinsically hydrophilic nature of the polymeric matrix, rather than with defects arising from the fabrication process.[41] The PVA/PAA system, being water-soluble, exhibits a high moisture absorption capacity; in this context, the incorporation of CDs, which are rich in oxygen-containing functional groups, can promote localized water uptake, inducing slight swelling within the polymer matrix.[41,42]

This phenomenon manifests as subtle surface roughness or the formation of microdomains without compromising the membrane's continuity or mechanical integrity. Similar morphologies associated with swelling processes have been widely reported in hydrophilic polymer systems reinforced with CDs, where these nanomaterials act as water-retention sites through hydrogen-bonding interactions.[41,43] In contrast, this behavior is not observed in PPSU-based membranes, owing to the hydrophobic and structurally rigid nature of this polymer, which limits water absorption and suppresses swelling effects.[44,45]

The morphological comparison following the addition of CDs reveals microstructural changes and pore formation in the polymeric matrix, as observed by SEM. In the pristine PPSU membrane (Fig. 3b), a homogeneous surface is observed, with circular-to-oval pores with average diameters of 0.01–0.06 μm, consistent with the typical structure of membranes fabricated *via* the phase inversion method using DMF as solvent,[46,47] which is consistent in the transversal section (Fig. 3d). This morphology reflects controlled demixing kinetics during membrane formation, which is favored by the hydrophobic nature of PPSU and the absence of hydrophilic additives. In contrast, the surface of PPSU-CDs (Fig. 3c) is rougher, with irregularly shaped pores and granular structures within the cavities, which can be attributed to partial aggregation of CDs or to their anchoring within the matrix during solidification. A higher density of interconnected microcavities is also observed in the transversal section (Fig. 3e), suggesting that the incorporation of CDs (rich in oxygenated and hydroxyl functional groups) alters the thermodynamics of the polymeric phase, accelerating the polymer/solvent demixing process and promoting a more porous morphology.[48] The presence of CDs not only affects the material's physical microstructure but may also influence its functional properties. The increase in roughness and the formation of microaggregates within pores can enhance the adsorption of ionic or dye species and improve light–matter interactions in photoactive processes. Moreover, the modification of surface topography may increase the membrane's hydrophilicity and, consequently, improve permeate flux and fouling resistance.[49,50]

Table 1 shows the porosity (ε) values calculated using the gravimetric method for the fabricated membranes. In all cases, the wet weight exceeded the dry weight, confirming proper water absorption and accurate determination of pore volume. The PVA/PAA membranes exhibited the highest porosity (90.15%), followed by PVA/PAA-CDs (91.58%), whereas the PPSU membranes showed lower values (82.70–84.24%). This difference is attributed to the greater hydrophilicity of the PVA/PAA system, in which the –OH and –COOH groups enhance water uptake and matrix swelling. The incorporation of CDs slightly increased porosity in both systems, an effect associated with the formation of microvoids and the presence of oxygenated groups in the CDs, which improve water affinity.[51] Compared with the obtained values (>80%), which are characteristic of highly porous membranes, the values are advantageous for applications requiring high permeability or efficient species diffusion, such as dye photodegradation processes or ion transport in catalytic and antimicrobial systems. The difference between PPSU and PVA/PAA also aligns with the expected morphological observations: the PVA/PAA system tends to exhibit a rougher surface with microdomains, whereas PPSU forms a more compact and less swellable matrix.[52,53]

Membrane thickness is a key parameter influencing both photocatalytic and antibacterial performance. Although it was not systematically varied in this study, its effects can be understood from transport and light interaction principles. Thinner membranes favor light penetration and enhance interaction between the active surface and pollutants,

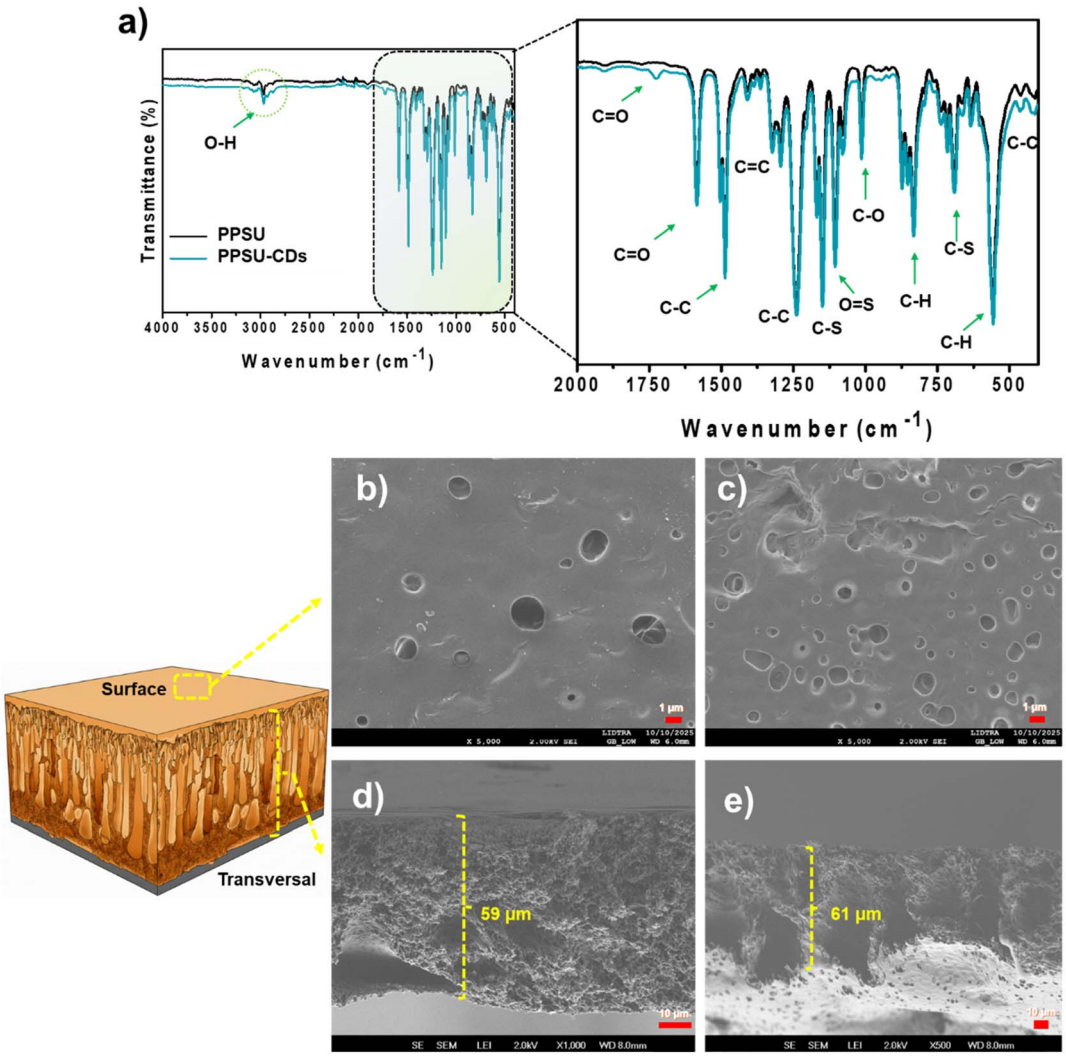

Fig. 3 Chemical and morphological characterization of PPSU membranes and the effect of CD incorporation. (a) FTIR spectra showing changes in functional groups after CD addition. (b and c) Surface SEM images of pristine PPSU and PPSU-CDs membranes, respectively, highlighting pore structure and surface roughness. (d and e) Cross-sectional SEM images showing internal morphology and pore distribution.

improving photocatalytic efficiency. In contrast, thicker membranes may hinder light transmission and limit access to reactive sites, although they offer better mechanical stability.[54–56]

Regarding antibacterial activity, thickness can affect both the contact between the membrane and bacterial cells and the diffusion of reactive species such as ROS. Therefore, optimizing membrane thickness is essential to balance structural stability and functional performance in future studies.[57]

3.3. Photodegradation test of nanostructured membranes

To evaluate the photodegradation capability of PVA/PAA-CDs membranes, two types of tests were conducted: one under

Table 1 Porosity percentage values of PPSU and PVA/PAA membranes and the effect of the CDs incorporation, calculated by gravimetry

	Wet weight (g)	Dry weight (g)	Polymer density (g cm^{-3})	Water density (g cm^{-3})	Porosity (%)
Membrane	w_1	w_2	d_p	d_w	ε
PPSU	0.0404	0.0087	1.31	0.998	82.7073
PPSU-CDs	0.035	0.0069	1.31	0.998	84.2411
PVA/PAA	0.0578	0.0071	1.28	0.998	90.1561
PVA/PAA-CDs	0.0711	0.0075	1.28	0.998	91.5798

direct solar irradiation (Fig. 4a, c, and e) and another under complete darkness (Fig. 4b, d, and f), aiming to discern the specific contribution of solar light to the degradation process by submerging the membranes in MB solutions. The system's evolution was calculated through both UV-Vis spectroscopic analysis and photographic recording. Fig. 4a presents the photodegradation rates of the membranes. From the first day of exposure, a noticeable decrease in blue color intensity was observed, particularly in solutions with initial MB concentrations of 2 and 4 ppm, as evidenced by the vial photographs (Fig. 4c). This visual change correlates with the progressive decrease in the characteristic absorption band of the dye (Fig. 4e), suggesting an initial adsorption process on the membrane, evidenced by the transition from a transparent to a blue hue. By the third day, the vials containing 2, 4, and 6 ppm solutions appeared nearly colorless, whereas those containing 8 and 10 ppm retained a faint blue hue. Nevertheless, by the seventh day, all vials appeared visually transparent, which was

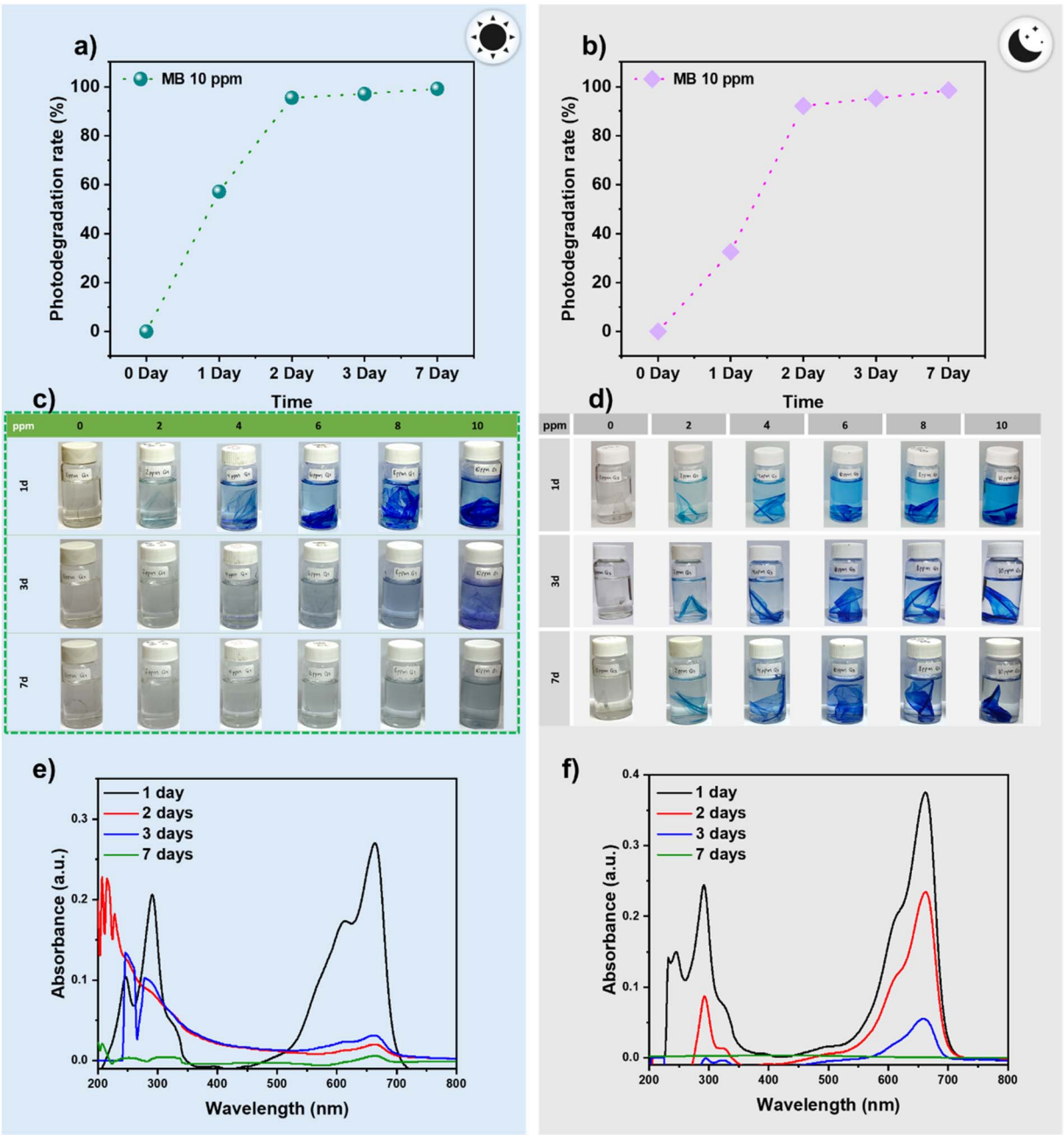

Fig. 4 Photodegradation performance of PVA/PAA-CDs membranes in methylene blue (MB) solutions under different conditions. (a) Degradation rate under solar irradiation. (b) Control experiment in dark conditions. (c and d) Photographs of MB solutions at different concentrations showing color evolution under light and dark conditions, respectively. (e and f) UV-Vis absorption spectra recorded at different times, demonstrating dye degradation under irradiation and adsorption behavior in darkness.

corroborated by the near-complete disappearance of the methylene blue absorption band in the UV-Vis spectra, thereby confirming efficient solar-induced photodegradation. The photodegradation of methylene blue (MB) using polymeric membranes based on PVA/PAA relies on the immobilization of photocatalysts or active groups within the polymeric matrix to induce redox processes under light irradiation, thereby oxidizing or cleaving the dye's molecular bonds. The membrane functions both as a stabilizing support and as a diffusion medium: MB molecules adsorbed on the polymeric surface remain in close proximity to active sites, where photon absorption generates electron–hole pairs that promote the formation of hydroxyl radicals, which subsequently oxidize MB to its mineralized products.[58] This mechanism is supported by the UV-Vis spectra (Fig. 4e), in which the characteristic absorption band is completely reduced after seven days of irradiation.

The results obtained under dark conditions (Fig. 4b, d and f) show a persistent coloration in the vials throughout the experiment. Although the water appeared transparent at the end of the test, the dye remained retained within the membrane, indicating that the process was limited solely to adsorption. The comparison between the two experimental conditions demonstrates that solar irradiation not only facilitates the visible removal of the dye from the solution but also promotes its effective degradation, thereby validating the photocatalytic degradation mechanism driven by light exposure.

Yan *et al.*[59] fabricated PVA/PAA nanofiber membranes *via* electrospinning, followed by a polydopamine (PDA) coating. Their results showed that the membrane adsorbed more than 93% of MB within 30 minutes, demonstrating a strong affinity for the dye. Although the primary focus of their study was adsorption rather than photodegradation, the authors suggested that the polymer-supported structure could subsequently serve as a platform for incorporating photocatalysts (*e.g.*, metal or semiconductor nanoparticles) to induce light-driven degradation. They also discussed the mechanical stability of the membranes after multiple adsorption/desorption cycles and the retention of the fibrous structure, critical aspects when considering their use as supports for photoactive degradation. Shamy *et al.*[60] demonstrated that, in PVA/QDs nanocomposite films, the incorporation of carbon dots within a hydrophilic PVA matrix not only induces modifications in surface morphology but also imparts additional functionalities to the material. In their study, the authors concluded that glucose-derived CDs serve as active phases, significantly enhancing the system's optical and catalytic properties, particularly for dye removal in aqueous media. This behavior was attributed to the high density of oxygen-containing functional groups on the CDs' surface and to their homogeneous dispersion within the polymer matrix.

Furthermore, it was reported that the presence of CDs induces local structural changes in PVA, primarily associated with physical interactions, such as hydrogen-bond formation, that promote water uptake and may lead to controlled swelling in water-soluble matrices. This effect accounts for the emergence of slight surface textural variations without compromising the material's continuity or mechanical integrity. Our findings on the use of the biodegradable PVA/PAA combination in water treatment have received limited attention due to its water solubility. However, this characteristic may confer an environmental advantage, as both polymers are biodegradable and, through induced crosslinking, can enhance membrane stability, enabling the development of more sustainable membranes with a lower ecological footprint.

As part of the comparative study, an analogous experiment was conducted using a PPSU matrix to contrast performance, given that PPSU is widely employed in water filtration systems due to its excellent physical and mechanical properties.[61,62] Fig. 5 shows the photodegradation performance of PPSU-CDs membranes under similar conditions to the previous PVA/PAA membrane test. According to the degradation rate (Fig. 5a), from the third day of exposure, a significant decrease in the blue coloration of the solution was observed, accompanied by visible retention of the dye on the membrane. By the seventh day, both the solution and the membrane appeared transparent, indicating effective degradation of MB, as evidenced by the color change in the vials (Fig. 5c) and reflected in the UV-Vis spectra (Fig. 5e). Additionally, the reusability performance of PPSU-CDs was determined after five cycles, demonstrating that the nanostructured membrane maintains their intrinsic photodegradation even after five cycles, as shown in the SI (S2).

In contrast, under dark conditions, the adsorption process in the PPSU-CDs membranes occurs more slowly and remains incomplete, as presented in Fig. 5b. Although a slight decrease in color intensity is observed by the seventh day, the solution still retains a noticeable blue coloration (Fig. 5d). This behavior suggests differences in adsorption capacity between the polymer matrices (PVA/PAA and PPSU). Unlike the PVA/PAA-CDs membranes, which under dark conditions can completely remove the dye from the liquid medium, the PPSU-CDs membranes exhibit considerably lower adsorption efficiency in the absence of light, highlighting the critical influence of the polymeric matrix on the overall performance of the system.

According to our results, the implementation of PPSU-based membranes as a functional support for the photodegradation of MB represents a promising strategy for water purification, owing to the inherent thermal robustness, chemical stability, and excellent mechanical strength of PPSU.[63,64] The incorporation of photocatalytic nanostructures into PPSU membranes has been previously reported. According to Dai *et al.*,[65] a mixture of rGO/TiO_2 nanoparticles was introduced into the PPSU matrix *via* a phase inversion process, yielding hybrid membranes that exhibited both photodegradation and self-cleaning capabilities under visible light. The results demonstrated that the synergy between rGO and TiO_2 nanomaterials enhances electron–hole pair separation, resulting in a significant increase in photocatalytic activity relative to PPSU membranes containing only GO or only TiO_2. In addition, Gan *et al.*[66] fabricated PPSU membranes modified with CDs/Ag nanofillers for the removal of tartrazine, demonstrating that incorporating CDs into sulfonated aromatic polymers is a viable strategy for photocatalytic degradation. In both cases, the membrane structure facilitates solid–liquid separation, enables reusability, and

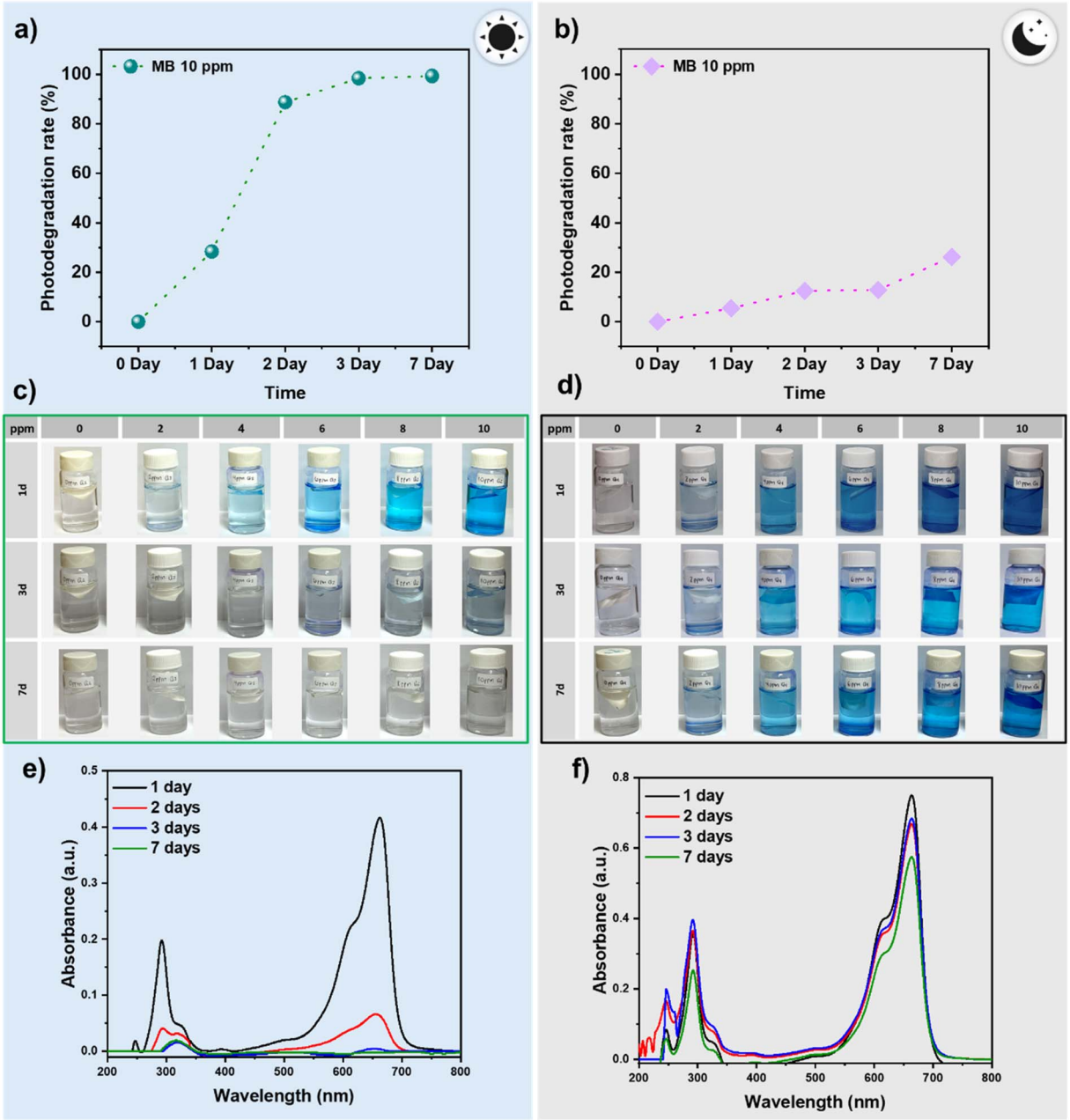

Fig. 5 Photodegradation performance of PPSU-CDs membranes in methylene blue (MB) solutions. (a) Degradation rate under solar irradiation. (b) Degradation behavior under dark conditions. (c and d) Visual evolution of MB solutions at different concentrations under light and dark conditions. (e and f) UV-Vis spectra showing the decrease in MB characteristic absorption band over time.

enhances overall efficiency by increasing contact between the reactant and the catalytic surface, thereby accelerating degradation kinetics.

The plots of $\ln(A_0/A_t)$ *versus* time (Fig. 6a and b) showed an almost linear behavior in the initial stages of the process, indicating that the degradation follows apparent pseudo-first-order kinetics. However, deviations from linearity at longer times suggest contributions from additional processes, such as adsorption and the formation of intermediates; that is, both adsorption and photodegradation are present, which is why the behavior is not 100% linear.

The obtained rate constants were 0.0434 h^{-1} for PVA/PAA-CDs and 0.0562 h^{-1} for PPSU-CDs with R^2 values of 0.9470 and 0.9715, respectively. The PVA/PAA-CDs membrane exhibited a higher apparent rate constant than that of the PPSU-CDs membrane, indicating faster MB removal under the tested conditions. However, this apparent kinetic behavior likely includes contributions from both adsorption and photocatalytic degradation, especially during the initial stages.

Free radical scavenging experiments were performed using isopropanol (IPA) to evaluate the role of hydroxyl radicals and thus validate ROS generation. Interestingly, the addition of IPA

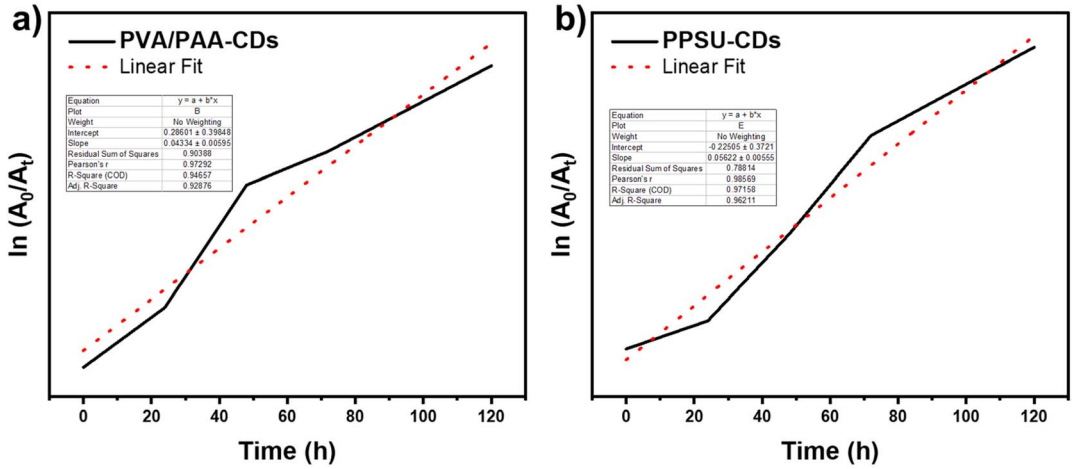

Fig. 6 First-order kinetics plots for MB degradation, (a) PVA/PAA-CDs and (b) PPSU-CDs.

led to an increase in degradation efficiency, suggesting that $^{\bullet}OH$ is not the dominant reactive species in this system.[67] The observed increase in degradation efficiency may be attributed to a shift in the reaction pathway, in which alternative reactive oxygen species, such as superoxide radicals or singlet oxygen, play a more significant role.[68] This behavior can be attributed to IPA's role as a hole scavenger, which reduces electron–hole recombination and enhances charge separation, thereby promoting electron-driven pathways, such as the formation of superoxide radicals. Similar effects have been reported in photocatalytic systems where the presence of hole scavengers improves photocatalytic efficiency by increasing the availability of reactive electrons and alternative oxidative species[69,70] (see SI).

3.4. Photodegradation mechanism by chemical oxygen demand (COD) monitoring

COD measurements were performed to monitor changes in total organic matter during the degradation of MB dye using PVA/PAA-CDs and PPSU-CDs membranes over four weeks. This technique enables evaluation of the total number of available electrons in the solution during dye degradation (mineralization), distinguishing between simple chromophore rupture and complete molecular oxidation.[71–73] Higher COD removal values suggest advanced oxidation processes of MB, attributable to the enhanced oxidant efficiency provided by the addition of CDs. However, low COD values indicate partial degradation, as evidenced by apparent decoloration, in which only the chromophore's aromatic structure is disrupted, while the subproducts remain. Fig. 7 shows the comparison of the COD percentage between PVA/PAA-CDs and PPSS-CDs membranes. In particular, PVA/PAA-CDs demonstrate COD removal approaching 100% from the first week, with a further *ca.* 94% removal after 4 weeks, indicating complete oxidation of the organic MB dye *via* molecular rupture, forming other oxidized species. In contrast, PPSU-CDs exhibit high initial COD removal (approximately 100% in weeks 1 and 2), followed by a decrease of approximately 82% in weeks 3 and 4. Although the addition of CDs was effective in the early stages, they remain intermediate MB subproducts in aqueous solution, indicating slight degradation with increasing exposure time. The differences in results among the polymer membranes could be attributed to the intrinsic properties of the polymers employed. The gradual release of PVA/PAA and CDs into the water, due to their high hydrophilicity,[74,75] contributes to the non-decreasing COD value observed over time. This characteristic is environmentally favorable, as PVA/PAA is a biocompatible and non-toxic polymer.[76] However, the insolubility of PPSU in aqueous media,[77] is due to its high tolerance for non-organic solvents (water). This characteristic ensures that the polymer is not continuously released, unlike in PVA/PAA.

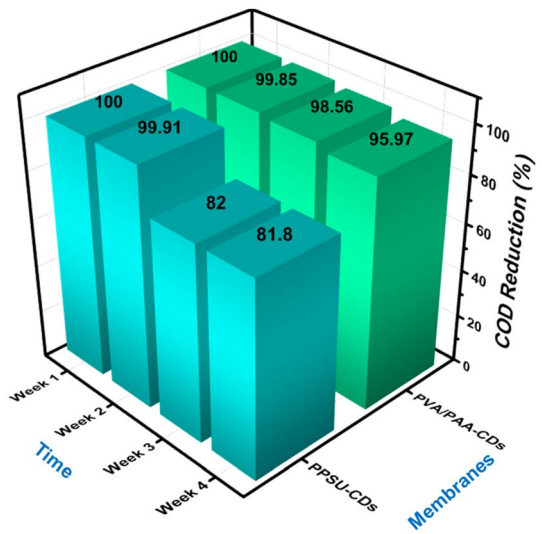

Fig. 7 Chemical oxygen demand (COD) removal efficiency during methylene blue (MB) degradation using PVA/PAA-CDs and PPSU-CDs membranes over four weeks. COD values indicate the degree of organic matter oxidation, allowing differentiation between partial degradation and advanced oxidation processes.

3.5. Bactericidal performance of nanostructured membranes

The development of nanostructured membranes for water treatment requires the rational design of multipurpose systems capable of simultaneously addressing dyes and pathogenic microorganisms that pose risks to human health. In this context, the incorporation of CDs as antimicrobial nanomaterials within polymeric matrices has been shown to reduce pathogenic load in aqueous environments.[78–80] Fig. 8 shows the antibacterial activity of PVA/PAA-CDs and PPSU-CDs against *P. aeruginosa* (Fig. 8a) and *S. aureus* (Fig. 8b), and their comparison with CDs suspension (5 mg mL^{-1}). As expected, the sole CD suspension exhibited bactericidal activity of approximately 99.99%. Regarding the CD-functionalized membranes, both showed significantly higher antimicrobial activity than their non-functionalized counterparts, which exhibited almost negligible bactericidal activity. After 3 hours of exposure, both the PVA/PAA-CDs and PPSU-CDs membranes achieved inhibition rates above 75%. After 24 hours, efficacy exceeded 97% in both cases, indicating progressive and sustained antibacterial activity. These results highlight the potential of CD-functionalized membranes as active materials for applications requiring continuous removal of microorganisms, such as contaminated water treatment or the protection of surfaces exposed to infectious agents.

The antibacterial performance of the developed membranes shows a clear time-dependent behavior, with moderate inhibition observed at early stages (1–3 h) and significantly enhanced bactericidal activity after 24 h of contact. This trend suggests that the antimicrobial effect is governed by a progressive mechanism, likely associated with the sustained generation of reactive species and prolonged interaction between the membrane surface and bacterial cells.

Additionally, the similar inhibition trends observed for both *Staphylococcus aureus* and *Pseudomonas aeruginosa* indicate that the antibacterial activity of CD-functionalized membranes is not strongly dependent on cell wall structure, suggesting a non-selective oxidative mechanism. This behavior is consistent with ROS-mediated antibacterial processes, where oxidative stress induces membrane damage, protein denaturation, and eventual cell death.[81] Notably, similar antibacterial trends were observed for *S. aureus* and *P. aeruginosa*, confirming that the CD-functionalized membranes exhibit consistent performance against both Gram-positive and Gram-negative bacteria. The sustained antibacterial effect observed over time further supports the role of prolonged membrane–bacteria interaction and ROS-mediated mechanisms in achieving high inhibition efficiency.

The results obtained against *S. aureus* (Fig. 8b) were comparable to those observed for *P. aeruginosa* (Fig. 8a). In both cases, the membranes modified with CDs exhibited significantly higher bactericidal activity than those composed solely of the base polymer, whose antimicrobial effect was practically negligible. After 3 hours of exposure, the membranes achieved bacterial inhibition levels above 80%. However, after 24 hours of contact, all CDs-functionalized membranes reached a bactericidal efficacy of 99.9%, confirming their long-term effectiveness. This behavior suggests that, upon incorporating CDs into the polymeric matrix, the direct contact area with microorganisms may be reduced relative to that of CDs in solution. Nevertheless, this initial limitation is offset by a sustained antimicrobial effect over time, reinforcing the potential of these membranes as active systems for applications requiring progressive and continuous pathogen removal, such as contaminated aquatic environments or prolonged-contact surfaces.[64,82]

The enhanced performance of CD-functionalized membranes can be attributed to the photoactive properties of carbon dots and their ability to ROS under light irradiation. Upon light absorption, CDs can undergo electronic excitation, promoting electrons from the valence band to higher-energy states and generating electron–hole pairs.[83] These charge carriers participate in redox reactions at the membrane

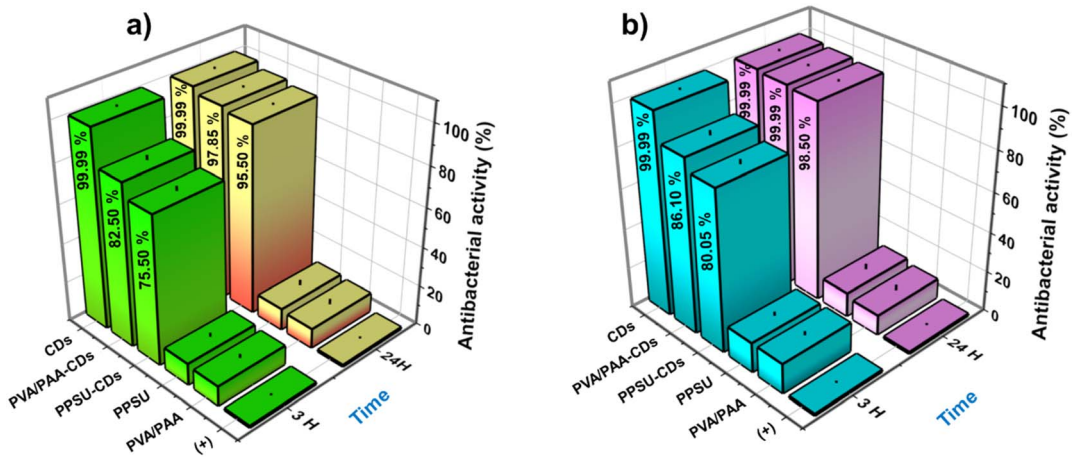

Fig. 8 Antibacterial activity of nanostructured membranes incorporating CDs against (a) *Pseudomonas aeruginosa* and (b) *Staphylococcus aureus*. The results show inhibition percentages at different contact times, highlighting the enhanced bactericidal performance of CD-functionalized membranes compared to pristine polymers.

interface, where photogenerated electrons reduce dissolved oxygen to form superoxide radicals, while holes oxidize water or hydroxyl ions to produce hydroxyl radicals. Additionally, energy transfer processes may lead to the formation of singlet oxygen.[84,85] These ROS play a crucial role in the oxidative degradation of methylene blue by cleaving chromophoric structures and forming smaller intermediate species, thereby contributing to advanced oxidation processes.[86] Simultaneously, ROS mediate antibacterial activity by inducing oxidative stress in microbial cells, leading to lipid peroxidation, protein damage, and disruption of cellular membranes.[87] Furthermore, the presence of nitrogen- and oxygen-containing functional groups on the surface of CDs introduces defect states that facilitate charge separation and enhance ROS generation.[88] These functional groups also promote strong interactions with the polymeric matrix and improve contact with bacterial cells, thereby amplifying both photocatalytic and antibacterial performance.

The use of CDs as an antimicrobial additive in polymer membranes has been described by different authors. Latif *et al.*[37] investigated the incorporation of undoped CDs into PVA matrices to enhance mechanical properties and reported antibacterial activity in the resulting composites. Beyond mechanical reinforcement, the authors noted that the presence of CDs imparted antibacterial properties to the composites, although extensive microbiological evaluations were not conducted. Similarly, Alaş *et al.*[36] incorporated multicolor CDs into PVA films and evaluated their antimicrobial activity. The composites exhibited notable activity against both Gram-positive and Gram-negative bacteria in qualitative assays and inhibited biofilm formation. The antibacterial action was primarily attributed to interactions between CDs and the bacterial cell surface, as well as to the generation of reactive species and the blocking (or interference) effect on bacterial adhesion. Zhao *et al.*[89] reported the synthesis of PVA composite films incorporating CDs and evaluated their antibacterial activity against *E. coli* and *S. aureus*. It was observed that pure PVA exhibited no antibacterial activity, whereas incorporating CDs into the composite films resulted in significant inhibition of bacterial growth, as evidenced by colony-forming unit (CFU) reduction assays. In contrast, no studies were found reporting antibacterial activity using PPSU as the polymeric matrix; however, similar work has been conducted with polysulfone (PSF). For instance, Mahat *et al.*[49] incorporated biomass-derived CDs into PSF for forward osmosis membranes and observed that the addition of CDs enhanced the material's antibacterial activity. Specifically, bacterial diffusion assays revealed reduced microbial proliferation on the CD-modified membranes compared to the unmodified PSF membrane. On the other hand, Chen *et al.*[48] modified a PSF membrane with a CD-gold nanoparticle hybrid and reported that the resulting membrane achieved an antibacterial rate of up to 90% against *E. coli*. According to the authors, the bactericidal efficacy of CDs arises from surface heteroatoms on the carbon framework, which, upon interaction with the aqueous medium, promote the generation of ROS. These ROS induce oxidative stress and cause irreversible damage to the structural integrity of microorganisms. Based on the reported results, this antimicrobial effect appears to be independent of the microbial cell wall structure. Furthermore, the homogeneous incorporation of these nanostructures into polymeric matrices enables controlled release of reactive species, thereby promoting a sustained antibacterial effect at later contact (24 h).

To simulate a more realistic application scenario in which the nanostructured membrane is fully immersed in a contaminated medium, an additional experiment was designed by introducing a bacterial load of 10^8 CFU mL^{-1} in the presence of the MB dye, replicating the procedure used in the photodegradation (under light irradiation) at 1 and 24 h of contact, as presented in Fig. 9. After one hour of exposure, both CD-functionalized membranes exhibited a slight decrease in bactericidal efficiency compared with the non-immersed tests. In particular, the PPSU-CDs membrane achieved an inhibition rate of 65%, whereas the PVA/PAA-CDs membrane achieved 68%. This reduction is attributed to a possible competition between the dye photodegradation mechanism and the bactericidal action, which may partially limit the surface availability of CDs for interaction with microorganisms. However, after 24 hours of exposure, both membranes recovered high efficiency, achieving bactericidal activities of 90% for PPSU-CDs and 92% for PVA/PAA-CDs, respectively. These findings highlight that although the initial effect is moderately reduced, the antimicrobial functionality is maintained and even enhanced over time. Furthermore, these findings highlight the multifunctional capabilities of the developed membranes, demonstrating simultaneous efficiency in both organic pollutant degradation and microorganism removal, making them promising candidates for use in water treatment systems and surfaces exposed to biological contamination.

Although no reports were found in the available literature describing membranes comparable to those developed in this

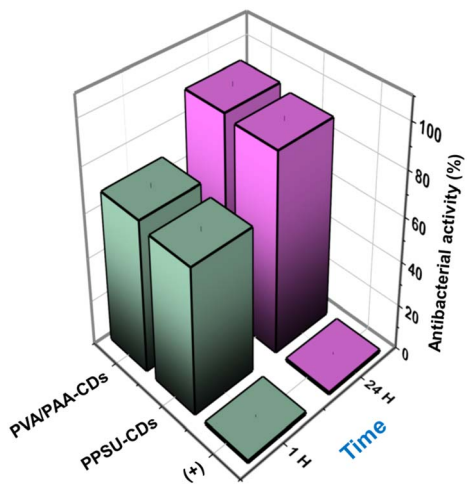

Fig. 9 Antibacterial activity of CD-functionalized membranes under combined conditions of methylene blue (MB) presence and light irradiation. Results show inhibition efficiency against *Pseudomonas aeruginosa* (10^8 CFU mL^{-1}) at different contact times, demonstrating the simultaneous functionality of photocatalytic and antibacterial processes.

work, Rasool *et al.*[90] prepared a CD-based material capable of simultaneously degrading Rhodamine B (RhB) and exhibiting antibacterial activity. Under irradiation, the system achieved efficient dye degradation while also inactivating bacteria present in the experimental environment, demonstrating that the ROS-mediated mechanisms responsible for dye degradation can likewise damage microbial cells. This study clearly validates the feasibility of a dual-action strategy, organic pollutant degradation coupled with antimicrobial activity within a single nanomaterial, thereby reinforcing the multifunctionality of our membrane under both scenarios. Zhao *et al.*[91] fabricated polylactic acid (PLA) nanofiber membranes incorporating nitrogen-doped carbon dots (N-CDs) and evaluated both contaminant degradation and antibacterial activity against *E. coli* and *C. albicans*. It was observed that the membrane containing approximately 8% N-CDs exhibited high photocatalytic efficiency for organic pollutants and significant simultaneous microbial inhibition. The results suggest that the presence of doped CDs enables effective ROS generation under irradiation, acting on both organic molecules and microorganisms within the same environment. Unlike the previously mentioned studies, the results reported here were obtained under direct exposure to natural sunlight rather than under controlled light irradiation. Despite this, excellent and representative results were obtained, comparable to those reported under artificial irradiation, without the need for any additional mechanical assistance. This finding suggests that our material can be effectively applied in harsh environments contaminated with both dyes and microorganisms. Owing to its multifunctional properties, it holds strong potential for applications in water treatment and purification systems.

From a practical perspective, the developed membranes exhibit strong scalability and reproducibility. The phase inversion method, widely used in industry, enables a straightforward transition from laboratory to pilot and industrial scales. Additionally, the synthesis of CDs *via* solution-based methods allows for large-scale, cost-effective production. Reproducibility is ensured through controlled preparation parameters such as polymer concentration, solvent composition, and CD loading, enabling consistent membrane properties. Furthermore, the use of stable polymer matrices like PVA/PAA and PPSU helps maintain structural integrity during operation. Overall, these features position CD-functionalized membranes as promising candidates for sustainable water treatment applications.

4. Conclusion

The present study demonstrates the successful fabrication of multifunctional polymeric membranes based on PVA/PAA and PPSU matrices incorporating green-synthesized CDs, providing an effective platform for simultaneous photocatalytic dye degradation and antibacterial activity. The integration of CDs into both polymeric systems enabled efficient removal of methylene blue under light irradiation, while also imparting strong bactericidal performance, confirming the dual functionality of the developed materials. The enhanced performance is attributed to the photoactive nature of CDs and their ability to generate reactive oxygen species (ROS), which govern both oxidative degradation and microbial inactivation. A comparative analysis revealed that PVA/PAA-CDs membranes exhibited superior adsorption capacity and slightly improved overall performance, whereas PPSU-CDs membranes provided higher structural stability, highlighting the critical role of polymeric environment in determining functional behavior. Importantly, this work advances the state of the art in CD-based photocatalytic systems by demonstrating a multifunctional, green-synthesized, and solar-driven approach that addresses both organic pollutants and microbial contamination on a single platform. These findings contribute to the development of sustainable water treatment technologies by integrating environmentally friendly materials with scalable fabrication methods. Future work should focus on optimizing CD composition through controlled doping strategies, evaluating long-term stability under real-world operating conditions, and investigating the influence of structural parameters, such as membrane thickness, on performance. Overall, this study provides a foundation for the design of next-generation smart membranes with enhanced efficiency and practical applicability in water remediation systems.

Author contributions

A. López-Amador: conceptualization, methodology, writing – original draft. P. Ortega-Sánchez: methodology. A. Y. Vázquez García: methodology, data curation. J. A. Díaz-Real: supervision, validation. A. J. Montes-Luna: resources, data curation. N. Arjona: resources, writing – review & editing. G. Luna-Bárcenas: writing – review & editing. B. L. España-Sánchez: funding acquisition, investigation, project administration, supervision, writing – review & editing.

Conflicts of interest

The authors declare that they have no competing financial interests or personal relationships that could have appeared to influence the work reported in this paper.

Data availability

Supplementary information (SI) is available. https://doi.org/10.1039/d6ra00999a.

The data supporting this article have been included in: https://drive.google.com/drive/folders/1G73Uhrec1ff9an6S2Q0m_wU1W9QiWiDR?usp=drive_link.

Acknowledgements

The authors thank SECIHTI and CIDETEQ for their support in completing this work through the PRONAII-90 2024 and MADTEC-110 2025 projects. The use of AI was employed exclusively for the spelling and grammar review of the original text.

References

1 P. O. Oladoye, T. O. Ajiboye, E. O. Omotola and O. J. Oyewola, *Results Eng.*, 2022, **16**, 100678.
2 V. Katheresan, J. Kansedo and S. Y. Lau, *J. Environ. Chem. Eng.*, 2018, **6**, 4676–4697.
3 R. Castellanos-Espinoza, N. Arjona and B. L. España-Sánchez, *Environ. Sci. Eng.*, 2025, **F65**, 119–138.
4 J. Saleem, Z. K. B. Moghal, S. Pradhan, A. Hafeez, M. Shoaib, J. Alahmad and G. McKay, *Polymers*, 2024, **16**, 1459.
5 P. V. Deepthi, K. Viji, A. M. Vijesh, A. M. Isloor and V. Kumar, *Advances in Separation Sciences: Sustainable Processes and Technologies*, 2025, pp. 227–250.
6 I. A. Khan, K. M. Deen, E. Asselin, M. Yasir, R. Sadiq and N. M. Ahmad, *J. Ind. Eng. Chem.*, 2025, **145**, 705–720.
7 S. Murugan and M. Ashokkumar, *Adv. Powder Technol.*, 2024, **35**, 104654.
8 B. M. Ibraheem, D. A. H. Al-Timimi, S. N. Abdullah, H. S. Majdi and Q. F. Alsalhy, *Chem. Eng. Res. Des.*, 2025, **218**, 312–327.
9 W. N. Wan Ishak, Y. P. Lim, N. F. Abu Bakar, L. Y. Ng and H. L. Tan, *J. Environ. Manage.*, 2026, **402**, 129134.
10 A. Zourou, A. Ntziouni, A. Karagianni, N. Alizadeh, N. Argirusis, M. Antoniadou, G. Sourkouni, K. V. Kordatos and C. Argirusis, *Inorganics*, 2025, **13**(9), 286.
11 M. D. Malitha, M. T. H. Molla, M. A. Bashar, D. Chandra and M. S. Ahsan, *Sci. Rep.*, 2024, **14**(1), 17976.
12 S. Shirazian, M. Rezakazemi, A. Marjani and M. S. Rafivahid, *Asia-Pac. J. Chem. Eng.*, 2012, **7**, 828–834.
13 H. Ren, A. Labidi, Z. Miao, J. Liang, X. Feng, M. Li, Y. Zhao and C. Wang, *Adv. Powder Mater.*, 2026, **5**, 100372.
14 H. Singh, A. Ahlawat, R. K. Sajwan and P. R. Solanki, *ChemistrySelect*, 2025, **10**, e01926.
15 T. Riaz, Z. A. Raza and Z. A. Rehan, *Chem. Afr.*, 2025, 1–18.
16 E. C. Wong, W. C. Chong, Y. L. Pang and Y. H. Ong, *J. Water Process Eng.*, 2025, **69**, 106698.
17 E. Fenelon, A. C. Ni'am, T.-M. T. Nguyen, Y.-F. Lin, Y.-F. Wang and S.-J. You, *J. Chem.*, 2023, **2023**, 8471214.
18 A. López-Amador, B. I. Jiménez-Muñóz, A. Gutierrez-Ortega, D. Eduardo Elizondo-Quiroga, G. Luna-Bárcenas, L. Gerardo Silva Vidaurri, M. Estevez and B. Liliana España-Sánchez, *Mater. Lett.*, 2024, **366**, 136569.
19 J. F. Li, Z. L. Xu and H. Yang, *Polym. Adv. Technol.*, 2008, **19**, 251–257.
20 M. D. Malitha, M. T. H. Molla, M. A. Bashar, D. Chandra and M. S. Ahsan, *Sci. Rep.*, 2024, **14**(1), 17976.
21 T. T. D. Nguyen, D. Nguyen, P. P. Vo, H. N. Doan, H. T. N. Pham, V. H. Hoang, K. Tien Le, K. Kinashi, V. T. Huynh and P. T. Nguyen, *J. Mol. Liq.*, 2023, **381**, 121831.
22 5220 Chemical Oxygen Demand (COD) - Standard Methods For the Examination of Water and Wastewater, DOI: 10.2105/SMWW.2882.103, accessed 16 September 2025.
23 L. Ren and K. Yang, *Metallic Foam Bone: Processing, Modification and Characterization and Properties*, 2017, pp. 203–216.
24 J. C. Kung, I. T. Tseng, C. S. Chien, S. H. Lin, C. C. Wang and C. J. Shih, *RSC Adv.*, 2020, **10**, 41202–41208.
25 R. Yang, X. Guo, L. Jia, Y. Zhang, Z. Zhao and F. Lonshakov, *Appl. Surf. Sci.*, 2017, **423**, 426–432.
26 H. Ding, P. Zhang, T. Y. Wang, J. L. Kong and H. M. Xiong, *Nanotechnology*, 2014, **25**, 205604.
27 N. A. Travlou, D. A. Giannakoudakis, M. Algarra, A. M. Labella, E. Rodríguez-Castellón and T. J. Bandosz, *Carbon*, 2018, **135**, 104–111.
28 S. Demirci, A. B. McNally, R. S. Ayyala, L. B. Lawson and N. Sahiner, *J. Drug Delivery Sci. Technol.*, 2020, **59**, 101889.
29 P. Surendran, A. Lakshmanan, S. S. Priya, K. Balakrishnan, P. Rameshkumar, K. Kannan, P. Geetha, T. A. Hegde and G. Vinitha, *Nano-Struct. Nano-Objects*, 2020, 100589.
30 Q. Liang, W. Ma, Y. Shi, Z. Li and X. Yang, *Carbon*, 2013, **60**, 421–428.
31 Q. Liang, W. Ma, Y. Shi, Z. Li and X. Yang, *Carbon*, 2013, **60**, 421–428.
32 G. Deme, A. Belay, D. M. Andoshe, G. Barsisa, D. Tsegaye, S. Tiruneh and C. Seboka, *J. Nanomater.*, 2023, **2023**, 1701496.
33 K. A. A. Mary, N. V. Unnikrishnan and R. Philip, *APL Mater.*, 2014, **2**, 076104.
34 F. Li, X. Jiang, J. Zhao and S. Zhang, *Nano Energy*, 2015, **16**, 488–515.
35 N. X. Chen and J. H. Zhang, *Chin. J. Polym. Sci.*, 2010, **28**, 903–911.
36 M. Ö. Alaş, G. Doğan, M. S. Yalcin, S. Ozdemir and R. Genç, *ACS Omega*, 2022, **7**, 29967–29983.
37 Z. Latif, H. B. Albargi, Z. Khaliq, K. Shahid, U. Khalid, M. B. Qadir, M. Ali, S. N. Arshad, A. S. Alkorbi, M. Jalalah and M. Jalalah, *Nanoscale Adv.*, 2024, **6**, 1750–1764.
38 N. A. Peppas and S. L. Wright, *Macromolecules*, 1996, **29**, 8798–8804.
39 N. A. Hamizi and M. R. Johan, *Mater. Chem. Phys.*, 2010, **124**, 395–398.
40 Z. W. Heng, Y. Y. Tan, W. C. Chong, E. Mahmoudi, A. W. Mohammad, H. C. Teoh, L. C. Sim and C. H. Koo, *J. Water Process Eng.*, 2021, **40**, 101805.
41 M. Li, Y. Du, J. Zhao, Y. Jiang, Y. Zhang and J. Yi, *Food Packag. Shelf Life*, 2026, **53**, 101701.
42 H. B. Ahmed, H. E. Emam and T. I. Shaheen, *Sci. Rep.*, 2024, **14**, 29226.
43 P. K. Pandey, Preeti, K. Rawat, T. Prasad and H. B. Bohidar, *J. Mater. Chem. B*, 2020, **8**, 1277–1289.
44 X. Chen, J. Zhang, X. Chen, Y. Zhu and X. Liu, *ACS Omega*, 2023, **8**, 10487–10492.
45 Y. Ma, L. Pan, K. Jiang, Q. Wang, Z. Zhu and Y. Tian, *Chem. Eng. J. Adv.*, 2023, **16**, 100557.
46 A. López Amador, A. F. Martínez Ávila, Z. P. Aranda Barrera, M. A. González Reyna, R. Castellanos Espinoza and B. L. España Sánchez, *Polym. Compos.*, 2023, **44**, 4309–4323.
47 Y. Yu, Q. Han, H. Lin, S. Zhang, Q. Yang and F. Liu, *J. Membr. Sci.*, 2022, **660**, 120872.
48 B. Chen, J. Zhang, Y. Zhang, L. Zhu and H. Zhao, *Nano*, 2020, **15**(10), 2050131.

49 N. A. Mahat, S. A. Shamsudin, N. Jullok and A. H. Ma'Radzi, *Desalination*, 2020, **493**, 114618.
50 P. G. Gan, S. T. Sam, M. F. bin Abdullah and M. F. Omar, *J. Appl. Polym. Sci.*, 2020, **137**, 48544.
51 S. Kiani, S. M. Mousavi, N. Shahtahmassebi and E. Saljoughi, *Appl. Surf. Sci.*, 2015, **359**, 252–258.
52 A. K. Shukla, J. Alam, M. Alhoshan, L. A. Dass and M. R. Muthumareeswaran, *Sci. Rep.*, 2017, **7**, 1–12.
53 A. Filimon, A. M. Dobos, M. D. Onofrei and D. Serbezeanu, *Polymers*, 2025, **17**, 1016.
54 R. W. Baker, *Membrane Technology and Applications*, DOI: 10.1002/9781118359686.
55 C. A. Smolders, A. J. Reuvers, R. M. Boom and I. M. Wienk, *J. Membr. Sci.*, 1992, **73**, 259–275.
56 S. Mozia, *Sep. Purif. Technol.*, 2010, **73**, 71–91.
57 S. A. Kousheh, M. Moradi, H. Tajik and R. Molaei, *Int. J. Biol. Macromol.*, 2020, **155**, 216–225.
58 V. Thamilselvan, S. Balu, D. Ganapathy, R. Atchudan, S. Arya, S. Hazra and A. K. Sundramoorthy, *Results Surf. Interfaces*, 2025, **19**, 100520.
59 J. Yan, Y. Huang, Y. E. Miao, W. W. Tjiu and T. Liu, *J. Hazard. Mater.*, 2015, **283**, 730–739.
60 A. G. El-Shamy and H. S. S. Zayied, *Synth. Met.*, 2020, **259**, 116218.
61 A. K. Shukla, J. Alam and M. Alhoshan, *Membranes*, 2022, **12**(2), 247.
62 O. Gronwald, I. Frost, M. Ulbricht, A. Kouchaki Shalmani, S. Panglisch, L. Grünig, U. A. Handge, V. Abetz, M. Heijnen and M. Weber, *Sep. Purif. Technol.*, 2020, **250**, 117107.
63 Y. R. Taha, A. Zrelli, N. Hajji, Q. Alsalhy, M. Rafiq and M. Irfan, *Can. J. Chem. Eng.*, 2025, **103**, 4456–4472.
64 A. López Amador, A. F. Martínez Ávila, Z. P. Aranda Barrera, M. A. González Reyna, R. Castellanos Espinoza and B. L. España Sánchez, *Polym. Compos.*, 2023, **44**, 4309–4323.
65 F. Dai, S. Zhang, Q. Wang, H. Chen, C. Chen, G. Qian and Y. Yu, *Front. Chem.*, 2021, **9**, 753741.
66 J. Y. Gan, W. C. Chong, L. C. Sim, C. H. Koo, Y. L. Pang, E. Mahmoudi and A. W. Mohammad, *Membranes*, 2020, **10**, 175.
67 B. C. Moon, B. Bayarkhuu, K. A. I. Zhang, D. K. Lee and B. Byun, *Energy Environ. Sci.*, 2022, **15**, 5082–5092.
68 A. Trenczek-Zajac, M. Synowiec, K. Zakrzewska, K. Zazakowny, K. Kowalski, A. Dziedzic and M. Radecka, *ACS Appl. Mater. Interfaces*, 2022, **14**, 38255–38269.
69 R. Palominos, J. Freer, M. A. Mondaca and H. D. Mansilla, *J. Photochem. Photobiol., A*, 2008, **193**, 139–145.
70 A. Chakraborty, A. Alam, U. Pal, A. Sinha, S. Das, T. Saha-Dasgupta and P. Pachfule, *Nat. Commun.*, 2025, **16**(1), 503.
71 Y. D. Hang, Determination of oxygen demand, *Food Analysis*, Springer, 2017, pp. 503–507.
72 S. Yang, H. He, D. Wu, D. Chen, X. Liang, Z. Qin, M. Fan, J. Zhu and P. Yuan, *Appl. Catal., B*, 2009, **89**, 527–535.
73 J. M. Herrmann, *Catal. Today*, 1999, **53**, 115–129.
74 R. R. Choudhury, J. M. Gohil and K. Dutta, *Iran. Polym. J.*, 2022, **31**, 1537–1550.
75 V. Kansay, V. D. Sharma, G. Chandan, I. Sharma, S. Chakrabarti and M. K. Bera, *Res. Chem. Intermed.*, 2025, **51**, 2605–2620.
76 J. Jose, F. Shehzad and M. A. Al-Harthi, *Polym. Bull.*, 2014, **71**, 2787–2802.
77 Y. Feng, G. Han, L. Zhang, S. B. Chen, T. S. Chung, M. Weber, C. Staudt and C. Maletzko, *Polymer*, 2016, **99**, 72–82.
78 B. Guo, G. Liu, C. Hu, B. Lei and Y. Liu, *Mater. Adv.*, 2022, **3**, 7726–7741.
79 X. Zeng, Z. Wang, N. Meng, D. T. McCarthy, A. Deletic, J. Hong Pan and X. Zhang, *Appl. Catal., B*, 2017, **202**, 33–41.
80 L. Wang, Z. Yuan, H. E. Karahan, Y. Wang, X. Sui, F. Liu and Y. Chen, *Nanoscale*, 2019, **11**, 9819–9839.
81 V. Takhar and S. Singh, *Environ. Sci. Nano*, 2025, **12**, 2516–2550.
82 M. M. Onica Hern Andez-Orozco, R. Castellanos-Espinoza, N. A. Hern Andez-Santos, F. A. B. Ramírez-Montiel, L. Alvarez-Contreras, V. M. Arellano-Arreola, F. Padilla-Vaca, N. Arjona and B. L. E.-S. Anchez, *Polym. Compos.*, 2023, **44**, 1711–1724.
83 S. Arif, S. Rasheed, N. Ahmad, M. I. Nabeel, W. Ahmad, T. Alomayri, D. Hussain and S. G. Musharraf, *J. Water Process Eng.*, 2026, **81**, 109274.
84 T. Yu, G. Jiang, R. Gao, G. Chen, Y. Ren, J. Liu, H. C. van der Mei and H. J. Busscher, *Mater. Adv.*, 2022, **3**, 7726–7741.
85 P. N. Dave and S. Chaturvedi, *ACS Symp. Ser.*, 2024, **1465**, 63–80.
86 S. Gengan, H. C. Ananda Murthy, M. Sillanpää and T. Nhat, *Results Chem.*, 2022, **4**, 100674.
87 N. H. Hussen, A. H. Hasan, Y. M. FaqiKhedr, A. Bogoyavlenskiy, A. R. Bhat and J. Jamalis, *ACS Omega*, 2024, **9**, 9849–9864.
88 S. M. Dizaj, A. Mennati, S. Jafari, K. Khezri and K. Adibkia, *Adv. Pharm. Bull.*, 2015, **5**, 19.
89 L. Zhao, M. Zhang, A. S. Mujumdar, B. Adhikari and H. Wang, *ACS Appl. Mater. Interfaces*, 2022, **14**, 37528–37539.
90 S. Rasool, M. Imran, A. Haider, A. Shahzadi, W. Nabgan, I. Shahzadi, F. Medina, M. M. Algaradah, A. M. Fouda, A. Al-Shanini and M. Ikram, *ACS Omega*, 2023, **8**, 25401–25409.
91 Y. Zhao, Y. Han, H. Zhang, B. Hu, S. Qu, C. Miao, L. Qin and G. Song, *Diamond Relat. Mater.*, 2025, **158**, 112612.